LAWRENCE
LIVERMORE
NATIONAL
LABORATORY

LLNL-JRNL-655940

Anomalous Radiochemical Recovery of Post-Detonation Gold Residues at the National Iginition Facility

P. Grant, K. Moody, N. Gharibyan, J. Despotopulos, A. Shaughnessy

June 17, 2014

Journal of Radioanalytical and Nuclear Chemistry

Disclaimer

Anomalous Radiochemical Recovery of Post-Detonation Gold Residues at the National Ignition Facility

Patrick M. Grant, Kenton J. Moody, Narek Gharibyan,
John D. Despotopulos, and Dawn A. Shaughnessy

Experimental Nuclear and Radiochemistry Group
Chemical Sciences Division
Livermore National Laboratory
Livermore, CA 94550
email: grant4@llnl.gov

Abstract Activated Au from a fragmented and dispersed NIF hohlraum is of interest to measure the induced 14.1-MeV $^{198m+g}$Au/^{196g}Au isotope ratio as an assessment of shot performance. A radiochemical recovery procedure, based on Au complexation by cyanide in NaOH-NaCN solution, was developed to reclaim radiogold (*Au) residues from post-detonation graphite collector foils. The average overall radiochemical yield from grafoils in an equatorial position relative to the hohlraum was 88%. However, the yield from the identical procedure applied to post-shot grafoils positioned axially (polar) was much decreased. The chemical dependency of explosion reaction products on collector position around an ostensibly symmetric fusion source is currently unexplained.

Keywords Inertial confinement fusion (ICF) • NIF post-detonation debris specimens • 14.1-MeV neutron reaction products • graphite foil collectors • cyanide solution chemistry • Au radiochemical recoveries • anomaly of NIF equatorial *vs* polar chemical behavior

Introduction

The National Ignition Facility (NIF) at Livermore National Laboratory produces bursts of 14.1-MeV D-T fusion neutrons via inertial confinement of an indirectly-driven implosion of a small target capsule (1-6). The 192 independent beams of (frequency-tripled) 350-nm laser light deliver up to 1.9 MJ of focused light inside an ~130-mg Au (or Au-U) cylindrical radiation cavity (hohlraum) positioned at the center of a 10-m-diameter target chamber. The hohlraum is typically 5-10 mm in diameter × 10-20 mm in length × 30-100 μm thick, absorbs 80-90% of the laser energy, and is the source of a near-Planckian x-ray bath that compresses a spherical, inertial-confinement-fusion (ICF) capsule fixed within its interior. Orientation of the experimental apparatus is such that the 3.1-mm-diameter laser entrance holes at both ends of the hohlraum point toward the vertical poles of the target chamber, while the hohlraum waist is positioned at the equator.

The ignition capsule is typically an ~2-mm-diameter, Si-doped, graded-density plastic (or high-density-carbon) ablator that has been cryogenically layered with equimolar D-T ice as thermonuclear fuel. The fuel layer is on the order of 70 μm thick, with mass ~190 μg, and it is held below the triple-point of D-T ice at a shot-time temperature of 18.6 K. Spherical implosion is induced by a symmetric, soft x-ray drive from the hohlraum that has achieved a peak radiation temperature of ~300 eV. The x-rays ablate the capsule and perform *PdV* work to compress the fuel assembly to high areal density (presently ~ 0.9 g/cm^2), with an ~10-keV central hot-spot of radius ~40 μm and ~8-μg mass, thereby inducing nuclear fusion and a ns-pulse of thermonuclear neutrons at bang-time. Although some D-D (2.45 MeV) and T-T (≤ ~9.5 MeV) neutrons are also produced, the dominant reaction is D-T to generate 14.1-MeV neutrons. NIF operating

parameters during the course of this work produced fluences of 10^{15}–10^{16} D-T neutrons (4π) per shot.

The Experimental Nuclear and Radiochemistry Group at Livermore fields various metal disks in the Solid Radiochemistry Collector (SRC) diagnostic to collect post-shot capsule and hohlraum debris in both the equatorial and axial (polar) directions (7). The principal metals used in this capacity were selected upon considerations of high melting point, minimum neutron activation, and reasonable cost, and thus far have included Ta, V, C, Nb, Ti, Ag, and Mo, all at high-purity and research-grade quality. The principal investigative analyte to date has been Au explosion debris, specifically radiogold (*Au) and the $^{198m+g}Au/^{196g}Au$ isotope ratio induced in the hohlraum by 14.1-MeV neutron activation (8). It has been shown that measurement of this *Au parameter [thereby delineating (n,γ) *vs* (n,2n) reaction products], in conjunction with the independently measured neutron down-scatter ratio (DSR) (5), can serve as a performance indicator for ablator compression and DT assembly confinement time during thermonuclear burn (8). It also has potential applications to fundamental research in nuclear physics and astrophysics.

Of the metal collectors, C (i.e., graphite foil or "grafoil") has particular appeal. It does not extensively or effectively activate [^{11}C $t_{½}$ = 20 min; no γ]; it is readily configured into arbitrary shapes; melts at > 2760°C; is available in high purity; and is economical. However, a standard method for reclaiming Au from simple solid surfaces, dissolution in aqua regia, is unsuccessful in quantitatively recovering *Au from post-detonation grafoil collectors. Typical aqua-regia radiochemical yields in our laboratory were on the order of only 5%, likely due to an affinity of $Au[Cl]_x$ [log K = 8.51–29.6 at 25° for x = 1-4 (9)] for active C of high surface area. Moreover, grafoil decomposes on contact with strong HNO_3, oxidizing to form bubbles of CO

and CO_2. Consequently, a more stable and efficient recovery procedure for *Au was developed. Quantitative chemical recovery, along with subsequent combining of *Au from multiple grafoils in a given experiment, were desired in order to sample, concentrate, and analyze a larger solid-angle of collection without overwhelming finite detector resources. The unsatisfactory yields from leaching with aqua regia led to exploration of the gold-cyanide complex, $Au[CN]_2^-$ (10) as a potential agent for the successful separation of *Au from NIF post-explosion debris on grafoil.

The commercial extraction of Au from mined ore (pulp), after leaching and coordination with cyanide, is the basis of the preferred international method for Au reclamation. This carbon-in-pulp (CIP) extraction process [sometimes carbon-in-leach; CIL (11)] is both inexpensive and simple to implement, and can convert a Au concentration of grams/ton in ore to a final bullion of ~100 wt.%. In one variant of CIP, finely sized raw ore is contacted with cyanide solution to produce soluble $Au[CN]_2^-$, following which larger particles of activated C are added to the slurry to sorb $Au[CN]_2^-$ with high efficiency. Filtration separates the C+Au agglomerates from the pulp, and Au is subsequently eluted from the C by treatment at high temperature and pH. Gold (along with any competing metals; e.g., Ag, Cu, Ni) is then precipitated at the cathodes of electrowinning cells. Additional purification may be accomplished by further smelting the cathode material, and, unsurprising for an industrial protocol developed for precious metal, the overall recovery of Au from ore is impressively quantitative [up to 97% (11)] and may achieve an ultimate purity of 99.999 wt.% in the refinery.

For the present application, however, adaptation of established commercial methods was not straightforward. First, complexation of the *Au with cyanide was unnecessary for its sorption by activated C, as it had already been deposited on (or embedded in) the grafoil by the NIF explosion. The primary interest in $*Au[CN]_2^-$ in this work was for elution of *Au from the

collector. Unfortunately, although many papers have been published about the $Au[CN]_2^-$ adsorption pathway on activated C, relatively little work has been done on elution mechanisms (12). Second, even after reaction with a cyanide solution to create $*Au[CN]_2^-$ for potential separation from the grafoil, this formation complex may be easily reabsorbed due to its own strong affinity for the substrate. Thus, in contrast to the industrial methods, the cyanide medium cannot be cleanly factored into disjoint adsorption and desorption tactics, leading to an adjustable rate of elution from the grafoil as an important experimental variable for this work.

The desorption of $Au[CN]_2^-$ from activated C may be influenced by several experimental conditions. Perhaps the most important factor is high temperature, as Au removal is known to vary directly with temperature, aided to some degree by decomposition of the cyanide chelator via hydrolysis at elevated temperature (12). Other easily adjustable empirical parameters affecting desorption include cyanide concentration, caustic concentration, total ionic strength, and Au concentration (11).

Experimental

Materials, Irradiations, and Data Analysis

Graphite foil of 0.13-mm thickness and 99.8% purity (metals basis) was obtained from Alfa Aesar. The foil had been strengthened with a thin metal laminate, and was mechanically cut into 5-cm-diameter targets for collections at a distance of 50 cm from an imploded fuel capsule positioned at the NIF target-chamber center (TCC). Partially masked behind a stainless-steel retaining ring, a grafoil collector presented an effective and direct line-of-sight exposure to TCC of 4-cm diameter for atomic and particulate ejecta from an explosion. Each grafoil thus subtended but 4×10^{-4} solid angle, and multiple grafoils were fielded at both polar and equatorial locations on an individual shot.

Following a NIF irradiation of 10^{15}-10^{16} (total) 14.1-MeV neutrons, each collector was mounted in a standard-geometry configuration for assays by nondestructive γ-ray spectrometry with 4096-channel MCA and HPGe systems. The *Au initially deposited on an individual collector foil was quantitatively measured through the γ-decays of 9.6-hour ^{196m}Au, 6.17-day ^{196}Au, and 2.69-day ^{198}Au. Spectral applications of photopeak energy, efficiency, and shape calibrations, as well as data analyses with incorporation of photon intensities, decay corrections, multiplicity correlations, and library identifications, were performed with the GAMANAL code (13). These initial NDA grafoil measurements comprised the absolute 100% *Au yield data for the ensuing radiochemistry development.

Radiochemistry

The experimental apparatus consisted of a 125-ml vacuum filter flask and glass microanalysis filter holder/chimney from Millipore Corp. The filter support was fritted glass, and a 0.45-μm JHWP (Teflon) filter was used to trap fine C particulates that would otherwise have passed into the flask with the eluent. After a NIF shot and the initial NDA *Au assay, the pliable grafoil collector (~ 0.25 – 0.3 g) was removed from its counting holder and curled around the interior wall of the filter chimney at its bottom. The 1.6-cm i.d. of the chimney perfectly accommodated the 5-cm grafoil without effective overlap, and the collection surface was always positioned to face inward toward the eluent flow (i.e., not in contact with the chimney wall).

Sequential 15-ml elutions of an irradiated grafoil were then performed, with the various experimental fractions collected in the flask and transferred into standardized solution-geometry counting vials for quantitative γ spectrometry. In conjunction with the prior NDA counting data, their assays allowed the direct calculation of stepwise radiochemical *Au yields, as well as an overall activity balance for a given experiment.

The only effective eluent realized in this work was a solution consisting of 1.5 M NaOH + 0.5 M NaCN, synthesized with AR-quality compounds, and preheated in a hot-water bath to a temperature of 97-98°C. The developed recovery process incorporates four such elutions for the quantitative removal of *Au. However, several other reagents were also considered and tested during this R&D phase in an effort to optimize the chemical yields. They included an industrial procedure of eluting with low-ionic-strength hot water (11); an alcohol elution; treatment with methylene chloride to dissolve and remove any potential organic binder from the grafoil; and a strong acid wash to remove any spectator cations known to form $M^{n+}(Au[CN]_2^-)_n$ ion-pairs on C, thereby suppressing elution of $Au[CN]_2^-$ (12). None of these tactics proved practically effective for this work, however, and none were consequently incorporated in the final procedure.

The four adopted elution steps were somewhat *ad hoc* and were developed through empirical testing of variables and variable combinations in controlled fashion. Constant for each elution was 15 ml of the NaOH/NaCN solution that had equilibrated within a hot-water bath at 97-98°C for ≥ 15 minutes. Variables were the presence of 0.5 mg of Au carrier in the eluent [or not; i.e., no carrier added (NCA)] and the rate of elution.

The desorption eluent flow was controlled only grossly via house vacuum through the sidearm of the flask. For this work, therefore, fast filtration through the Millipore system consisted of pouring the entire 15 ml of hot eluent into the filter chimney without applied vacuum, then opening the vacuum valve to full on. The total eluent contact and filtration time under these conditions was ~5 seconds. An intermediate contact time was attained by similarly pouring the 15 ml into the chimney in the absence of vacuum, waiting for 30 seconds, and then applying full vacuum (total residence time = 35 seconds). Slow elution was effected by pouring

the hot solution into the chimney and omitting the vacuum assist. Such filtration under only gravity flow required ~ 15-20 minutes to complete.

Thus, the developed, stepwise elution sequence consisted of the following procedures. As discussed later, the specific sequence of the steps in the protocol is important.

Eluent 1: NaOH/NaCN containing 0.5 mg Au carrier and fast elution

Eluent 2: NaOH/NaCN NCA with intermediate contact time

Eluent 3: NaOH/NaCN containing 0.5 mg Au carrier and slow elution

Eluent 4: NaOH/NaCN containing 0.5 mg Au carrier and slow elution (i.e., repeat #3)

Results and Discussion

The results of these development experiments are given in Table 1. They include the stepwise radiochemical yields, overall chemical yield, *Au remaining with the grafoil after the elutions, and the overall radioactivity balance for the experiments. Thus, for equatorial collectors, the instrumentally weighted average of 10 independent experiments gave a stepwise yield of (38 ± 7)% for Elution #1. The uncertainty assigned to a weighted average in this work was determined by the larger of two calculated variances: the uncorrected variance or the dispersion-corrected result (14). Different values of n were obtained for the various fractions of equatorial collection because of the iterative nature of the study. That is, since process modifications such as elution rate, eluent sequence, carrier *vs* NCA, and collateral solvent effects were investigated, not every trial mapped completely onto the final, 4-step protocol. However, when an individual measurement in an exploratory experiment was validly applicable to the optimum protocol, the datum was added to the results of the appropriate step measured in the ultimate procedure before final data processing.

The average overall *Au yield for equatorial collections was 88%, with 11% residual on the grafoil, and with an excellent radioactivity balance for the experiments of > 99%. The specific order and chemical composition of the four steps in this procedure is important. For example, switching steps 2 and 3 reduced the step-2 yield by ×2, while a similar reduction in step-3 recovery occurred if Au carrier was omitted from the NaOH-NaCN eluent. However, running eluent 4 as NCA seemingly had no effect on the (small) stepwise yield for that elution (but n = 1 only).

Although the sum of the average stepwise yields [(65 ± 8)%] overlaps the average overall yield [(88 ± 5)%] within their 2σ levels of confidence, it fails to do so at 1σ. This is attributed to the generally larger uncertainties in the stepwise average yields (16-22% RSD) compared to the RSD = 5% of the average overall yield. So while the distributions of the stepwise yields exhibited more variability and lower results in aggregate, any given complete experiment may be expected to reflect the 88% average overall yield more reliably. In the developed final procedure, therefore, it seemed that a loss of *Au from a given eluent volume (for whatever reason) was compensated by gain(s) in one or more of the other stepwise elutions. In this work, the average whole was greater than the average sum of its parts.

The situation for polar targets is very different, however. Our general experience has been that deposition of *Au on any metal collector at the polar position is appreciably less than what is obtained through equatorial collection on the same NIF shot. Fundamental outputs from a NIF explosion can be somewhat incongruous. For example, we measure the 14.1-MeV neutron fluence at both equatorial and polar positions via the $^{27}Al(n,\alpha)^{24}Na$ activation reaction on Al targets. Those results over the past three years indicate that neutron emission is reasonably isotropic, with any anisotropy between pole and equator being < 5%. Moreover, with n = 28

independent measurements, the $^{196m/g}$Au production ratios agree among themselves within 4%, and between the equatorial and polar collection positions to within 0.5% (15).

However, NIF photon output is less uniform. The x-ray hot spot presents an oblate shape when viewed from the equator, but a toroidal shape when viewed from a pole. This observation has been explained as toroid formation via a P4 Legendre mode on the ablator, induced by the lasers striking the hohlraum wall: the radiation drive at the waist of the implosion is slightly cooler than that experienced at the poles (5).

For post-shot hohlraum debris, the disparity between polar and equatorial distributions is both quantitatively and qualitatively striking in their differences. In addition to less efficient collection at the pole, the morphology of the ejecta is also quite different. For an equatorial collector, the physical appearance of grafoil is largely unchanged from its pre-shot appearance (see Figure 1). The *Au deposited equatorially would be consistent with an atomic vapor or mild chemical deposition following appreciable recoil thermalization. At the polar position, however, the explosion debris has a considerably harder component, with physical evidence for the presence of ballistic “chunks” readily detected by grafoil. Figure 2 shows micrographs of a post-shot polar grafoil collector from the same NIF experiment as Figure 1. The surface was generally more mottled, and mm-scale craters were produced in the collector by debris. Projectile penetration of the grafoil collector was complete in some instances, through not only the more fragile C layer, but also through its stiff metal backing.

As summarized in Table 1, the *Au grafoil chemical recoveries between pole and equator were very dissimilar as well. No attempt was made to optimize yields from the polar collectors, however; the Table-1 data reflect merely the application of the 4-step protocol for equatorial collection to polar grafoils. The first two eluents from a polar grafoil, rather than providing the

highest *Au stepwise yields, were relatively unworthy, while the majority of the recovered *Au was measured in eleunts 3 and 4. The average total recovery from polar collectors was but 24%, with a much higher fraction retained by the grafoil.

Explanations for this radiochemical anomaly are speculative at this time. The overall radioactivity balance for the polar experiments was (90 ± 4)%, reasonably good for such work, so loss of *Au through solution artifacts (e.g., unusual analyte plating or colloid formation) is not considered a major factor. Perhaps increased recoil energy at the pole embeds *Au deeper into the grafoil matrix, making it less accessible to effective contact by the NaOH-NaCN solvent (?). If so, a procedure incorporating a dry-ash of the polar grafoils may need development to improve those yields. Or perhaps there is a condition in the NIF target chamber, as yet unappreciated, that could be a contributing agent (?). For example, unconverted laser light ("glint") is known to be present at shot time, but its properties (such as intensity, isotropy, energy gradient, etc.) are largely speculative. This issue of anomalous NIF debris chemistry as a function of positioning around TCC is an open question at present.

Acknowledgements

The authors thank the NIF Nuclear Diagnostics Group and NIF Engineering and Operations staff, in particular, Richard Zacharias, Kenn Knittel, Christopher Wlodarczyk, Justin Wright, Bowdi Helgesen, Glenn Grant, Tim Cunningham, Wayne Abreu, James Daly, Bahram Talison, and the NIF Radiation Control Technicians. The assistance of Phil Torretto and Todd Wooddy in the LLNL Nuclear Counting Facility is also gratefully acknowledged. This work was performed under the auspices of the U.S. Department of Energy by Lawrence Livermore National Laboratory under Contract DE-AC52-07NA27344, and was funded by the Laboratory

Directed Research and Development Program at LLNL under project tracking code 13-ERD-036.

References

1. Haan SW, Lindl JD, Callahan DA, Clark DS, Salmonson JD, Hammel BA, *et al.* (2011) Point design targets, specifications, and requirements for the 2010 ignition campaign on the National Ignition Facility. Phys Plasmas 18: 051001

2. Landen OL, Edwards J, Haan SW, Robey HF, Milovich J, Spears BK, *et al.* (2011) Capsule implosion optimization during the indirect-drive National Ignition Campaign. Phys Plasmas 18: 051002

3. Edwards MJ, Lindl JD, Spears BK, Weber SV, Atherton LJ, Bleuel, DL, *et al.* (2011) The experimental plan for cryogenic layered target implosions on the NIF – the inertial confinement approach to fusion. Phys Plasmas 18: 051003

4. Dittrich TR, Hurricane OA, Callahan DA, Dewald EL, Doppner T, Hinkel DE, *et al*. (2014) Design of a high-foot high-adiabat ICF capsule for the NIF. Phys Rev Lett 112: 055002

5. Park H-S, Hurricane OA, Callahan DA, Casey DT, Dewald EL, Dittrich TR, *et al*. (2014) High-adiabat high-foot inertial confinement fusion implosion experiments on the NIF. Phys Rev Lett 112: 055001

6. Hurricane OA, Callahan DA, Casey DT, Celliers PM, Cerjan C, Dewald EL, *et al.* (2014) Fuel gain exceeding unity in an inertially confined fusion implosion. Nature 506: 343-348

7. Gostic JM, Shaughnessy DA, Moore KT, Hutcheon ID, Grant PM, Moody KJ (2012) Solid debris collection for radiochemical diagnostics at the National Ignition Facility (NIF). Rev Sci Instrum 83: 10D904

8. Shaughnessy DA, Moody KJ, Gharibyan N, Grant PM, Gostic JM, Torretto PC, *et al.* (2014) Radiochemical determination of inertial confinement fusion capsule compression at the NIF. Rev Sci Instrum, submitted

9. Smith RM, Martell AE (1976) Critical stability constants; vol. 4: inorganic complexes. Plenum Press, New York, p. 109.

10. Beck MT (1987) IUPAC critical survey of stability constants of cyano complexes. Pure Appl Chem 59: 1703

11. Metalliferous mining – processing / elution & carbon reactivation resource book. http://rsteyn.files.wordpress.com/2010/07/elution-and-carbon-reactivation-basics.pdf

12. Van Deventer JSJ, Van der Merwe PF (1994) The mechanism of elution of gold cyanide from activated carbon. Metall Mater Trans B 25: 829-838

13. Gunnink R, Niday JB (1971-1972) Computerized quantitative analysis by gamma-ray spectrometry. UCRL-51061, 5 volumes

14. ENSDF Nuclear Data Sheets (2014) General policies – "theory." p. iii http://indico.vecc.gov.in/indico/getFile.py/access?resId=0&materialId=6&confId=19

15. Gharibyan N, Moody K (2014) unpublished data

Table 1 Radiochemical distribution of *Au by NaOH-NaCN recovery procedure from NIF post-detonation grafoil collectors

Yields and Activity Balance (Uncertainties are 1σ)				
Experimental Fraction	**Equatorial Collection**	**n**	**Polar Collection**	**n**
Eluent 1	0.383 ± 0.070	10	0.0231 ± 0.0080	4
Eluent 2	0.139 ± 0.023	9	0.0311 ± 0.023	4
Eluent 3	0.105 ± 0.018	8	0.103 ± 0.042	4
Eluent 4	0.0266 ± 0.0057	4	0.144 ± 0.017	4
Grafoil Residual	0.108 ± 0.028	5	0.543 ± 0.081	4
Total Recovery	0.877 ± 0.047	5	0.245 ± 0.082	4
*Au Activity Balance	0.994 ± 0.015	6	0.901 ± 0.035	4

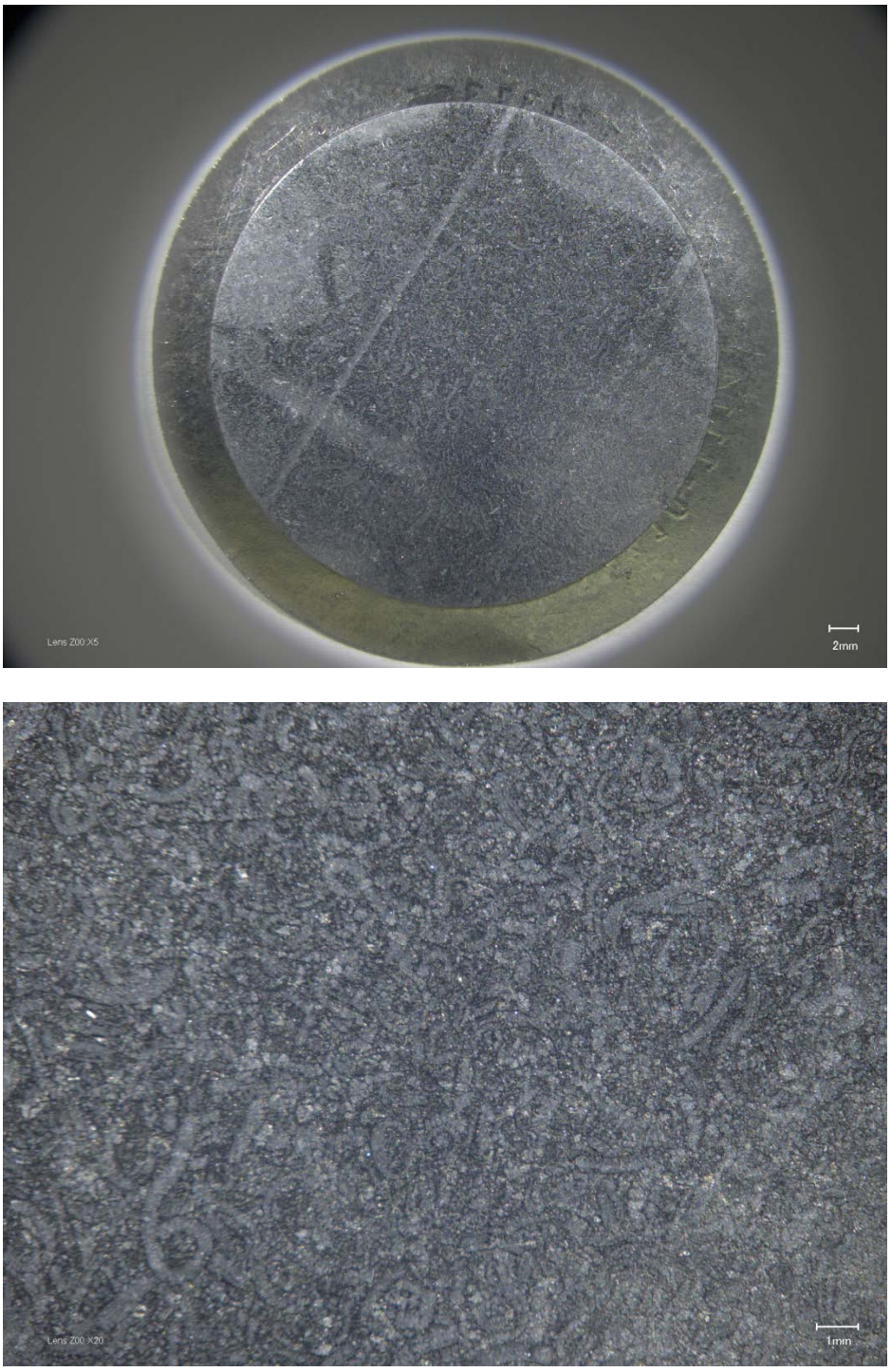

Fig. 1 Photomicrographs of post-shot equatorial grafoil collector #CUG66 from NIF shot N140225; top: 5×, bottom 20×

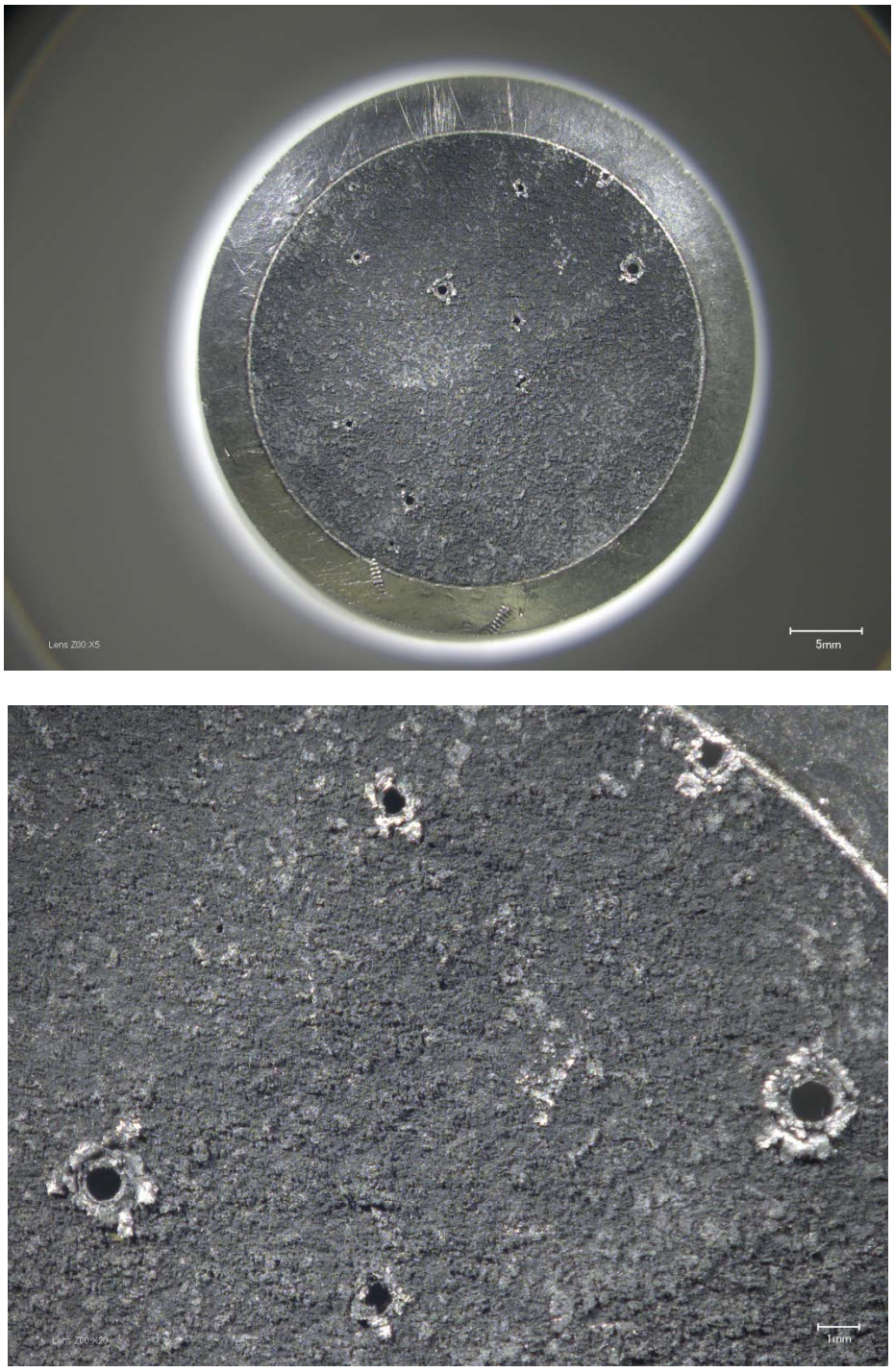

Fig. 2 Photomicrographs of post-shot polar grafoil collector #CUG35 from NIF shot N140225; top: 5×, bottom 20×